

# Extreme particle acceleration in the microquasar Cygnus X-3

M. Tavani<sup>1,2,3,4</sup>, A. Bulgarelli<sup>5</sup>, G. Piano<sup>1,4</sup>, S. Sabatini<sup>2,4</sup>, E. Striani<sup>2,4</sup>, Y. Evangelista<sup>1</sup>, A. Trois<sup>1</sup>, G. Pooley<sup>6</sup>, S. Trushkin<sup>7</sup>, N. A. Nizhelskij<sup>7</sup>, M. McCollough<sup>8</sup>, K. I. I. Koljonen<sup>9</sup>, G. Pucella<sup>10</sup>, A. Giuliani<sup>11</sup>, A. W. Chen<sup>3,11</sup>, E. Costa<sup>1</sup>, V. Vittorini<sup>1,3</sup>, M. Trifoglio<sup>5</sup>, F. Gianotti<sup>5</sup>, A. Argan<sup>1</sup>, G. Barbiellini<sup>3,12,13</sup>, P. Caraveo<sup>11</sup>, P. W. Cattaneo<sup>14</sup>, V. Cocco<sup>2</sup>, T. Contessi<sup>11</sup>, F. D'Ammando<sup>1,2</sup>, E. Del Monte<sup>1</sup>, G. De Paris<sup>1</sup>, G. Di Cocco<sup>5</sup>, G. Di Persio<sup>1</sup>, I. Donnarumma<sup>1</sup>, M. Feroci<sup>1</sup>, A. Ferrari<sup>3,15</sup>, F. Fuschino<sup>5</sup>, M. Galli<sup>16</sup>, C. Labanti<sup>5</sup>, I. Lapshov<sup>17</sup>, F. Lazzarotto<sup>1</sup>, P. Lipari<sup>18,19</sup>, F. Longo<sup>12,13</sup>, E. Mattaini<sup>11</sup>, M. Marisaldi<sup>5</sup>, M. Mastropietro<sup>20</sup>, A. Mauri<sup>5</sup>, S. Mereghetti<sup>11</sup>, E. Morelli<sup>5</sup>, A. Morselli<sup>4</sup>, L. Pacciani<sup>1</sup>, A. Pellizzoni<sup>21</sup>, F. Perotti<sup>11</sup>, P. Picozza<sup>2,4</sup>, M. Pilia<sup>21,22</sup>, M. Prest<sup>22</sup>, M. Rapisarda<sup>10</sup>, A. Rappoldi<sup>14</sup>, E. Rossi<sup>5</sup>, A. Rubini<sup>1</sup>, E. Scalise<sup>1</sup>, P. Soffitta<sup>1</sup>, E. Vallazza<sup>13</sup>, S. Vercellone<sup>23</sup>, A. Zambra<sup>3,11</sup>, D. Zanello<sup>18,19</sup>, C. Pittori<sup>24</sup>, F. Verrecchia<sup>24</sup>, P. Giommi<sup>24</sup>, S. Colafrancesco<sup>24</sup>, P. Santolamazza<sup>24</sup>, A. Antonelli<sup>25</sup> & L. Salotti<sup>26</sup>

Super-massive black holes in active galaxies can accelerate particles to relativistic energies<sup>1</sup>, producing jets with associated  $\gamma$ -ray emission. Galactic 'microquasars', which are binary systems consisting of a neutron star or stellar-mass black hole accreting gas from a companion star, also produce relativistic jets, generally together with radio flares<sup>2</sup>. Apart from an isolated event detected<sup>3</sup> in Cygnus X-1, there has hitherto been no systematic evidence for the acceleration of particles to gigaelectronvolt or higher energies in a microquasar, with the consequence that we are as yet unsure about the mechanism of jet energization. Here we report four  $\gamma$ -ray flares with energies above 100 MeV from the microquasar Cygnus X-3 (an exceptional X-ray binary<sup>4–6</sup> that sporadically produces radio jets<sup>7–9</sup>). There is a clear pattern of temporal correlations between the  $\gamma$ -ray flares and transitional spectral states of the radio-frequency and X-ray emission. Particle acceleration occurred a few days before radio-jet ejections for two of the four flares, meaning that the process of jet formation implies the production of very energetic particles. In Cygnus X-3, particle energies during the flares can be thousands of times higher than during quiescent states.

Cygnus X-3 (Cyg X-3) is a powerful X-ray binary that has a period<sup>5</sup> of  $P_{\text{orb}} = 4.8$  h and a typical luminosity near the maximum accretion power of a solar-mass compact star<sup>10</sup>,  $L_X \approx 10^{38}$  erg s<sup>-1</sup>, for a 10-kpc distance<sup>5</sup>. The compact star powering the system is either a neutron star in an unusual state of accretion or a black hole of 10–20 solar masses orbiting around a Wolf–Rayet companion star<sup>11</sup>. So far, emission up to  $\sim 300$  keV has been detected<sup>12,13</sup> from Cyg X-3 and usually shows a complex X-ray spectrum with two main states ('soft' and 'hard').

The Italian Space Agency's Astro-rivelatore Gamma ad Immagini Leggero (AGILE) satellite<sup>14</sup> dedicated a special programme of extensive pointings to the Cygnus region between mid 2007 and mid 2009. The

AGILE  $\gamma$ -ray instrument<sup>14</sup> is very compact and is capable of monitoring cosmic sources simultaneously in the  $\gamma$ -ray (0.1–10-GeV) and the hard-X-ray (18–60-keV) energy bands with good sensitivity and optimal angular resolution. AGILE operates in a fixed-pointing mode, implying that it can accumulate data on a source within its large field of view (2.5 sr for the  $\gamma$ -ray imager) fourteen times a day, taking into account Earth occultations during each spacecraft orbit. A typical one-day exposure above 100 MeV can reach  $10^7$  cm<sup>2</sup> s and is ideal for detecting microquasar variability on short timescales (as short as a few hours).

For Cyg X-3, AGILE accumulated a total exposure above 100 MeV of almost  $10^9$  cm<sup>2</sup> s (equivalent to an effective duration of about five months). The  $\gamma$ -ray intensity map of the Cygnus region is shown in Supplementary Fig. 1. This region is complex, hosting star formation sites, OB associations and several prominent X-ray sources. Galactic diffuse  $\gamma$ -ray radiation is taken into account by modelling<sup>15</sup> the interaction of cosmic rays with interstellar matter and radiation fields along the line of sight. AGILE's angular resolution satisfactorily resolves the field surrounding Cyg X-3 at  $\gamma$ -ray energies. A dominant source  $0.4^\circ$  from the Cyg X-3 position is the steady  $\gamma$ -ray pulsar<sup>16</sup> 1AGL J2032+4102/0FGL J2032.2+4122. By integrating all AGILE data, we find a weak ( $4.6\sigma$ )  $\gamma$ -ray source consistent with the position of Cyg X-3 and a flux of  $F = (10 \pm 2) \times 10^{-8}$  photons cm<sup>-2</sup> s<sup>-1</sup> above 100 MeV.

We also detect transient  $\gamma$ -ray emission from a flaring source consistent with the Cyg X-3 position, in four distinct episodes (Table 1; see also Supplementary Fig. 2). These flares were found in an independent multi-source maximum-likelihood search for transients in all available AGILE data (with off-axis angles less than  $45^\circ$ , and which covered an area of  $5^\circ \times 5^\circ$  centred at the Cyg X-3 position). The statistical significance of each flare was assessed using both the maximum-likelihood analysis and the false-discovery-rate<sup>17,18</sup> method. They all passed stringent post-trial

<sup>1</sup>INAF-IASF Roma, Via del Fosso del Cavaliere 100, I-00133 Roma, Italy. <sup>2</sup>Dipartimento di Fisica, Università Tor Vergata, Via della Ricerca Scientifica 1, I-00133 Roma, Italy. <sup>3</sup>Consorzio Interuniversitario Fisica Spaziale, Villa Gualino, Viale Settimio Severo 63, I-10133 Torino, Italy. <sup>4</sup>INFN Roma Tor Vergata, Via della Ricerca Scientifica 1, I-00133 Roma, Italy. <sup>5</sup>INAF-IASF Bologna, Via Gobetti 101, I-40129 Bologna, Italy. <sup>6</sup>Astrophysics Group, Cavendish Laboratory, 19 J. J. Thomson Avenue, Cambridge CB3 0HE, UK. <sup>7</sup>Special Astrophysical Observatory RAS, Karachaevo-Cherkassian Republic, Nizhnij Arkhyz 36916, Russia. <sup>8</sup>Smithsonian Center for Astrophysics, 60 Garden Street, Cambridge, Massachusetts 02138, USA. <sup>9</sup>TKK/Metsähovi Radio Observatory, Metsähovintie 114, Kylmälä 02540, Finland. <sup>10</sup>ENEA Frascati, Via Enrico Fermi 45, I-00044 Frascati (RM), Italy. <sup>11</sup>INAF-IASF Milano, Via E. Bassini 15, I-20133 Milano, Italy. <sup>12</sup>Dipartimento di Fisica, Università di Trieste, Via A. Valerio 2, I-34127 Trieste, Italy. <sup>13</sup>INFN Trieste, Padriciano 99, I-34012 Trieste, Italy. <sup>14</sup>INFN Pavia, Via Bassi 6, I-27100 Pavia, Italy. <sup>15</sup>Dipartimento di Fisica, Università di Torino, Via P. Giuria 1, I-10125 Torino, Italy. <sup>16</sup>ENEA Bologna, Via don Fiammelli 2, I-40128 Bologna, Italy. <sup>17</sup>IKI, Profsoyuznaya Street 84, Moscow 117997, Russia. <sup>18</sup>INFN Roma 1, Piazza Aldo Moro 2, I-00185 Roma, Italy. <sup>19</sup>Dipartimento di Fisica, Università La Sapienza, Piazza Aldo Moro 2, I-00185 Roma, Italy. <sup>20</sup>CNR, IMIP, I-00016 Montelibretti (Rome), Italy. <sup>21</sup>INAF Osservatorio Astronomico di Cagliari, Poggio dei Pini, I-09012 Capoterra (Cagliari), Italy. <sup>22</sup>Dipartimento di Fisica, Università Insubria, Via Valleggio 11, I-22100 Como, Italy. <sup>23</sup>INAF-IASF Palermo, Via La Malfa 153, I-90146 Palermo, Italy. <sup>24</sup>ASI Science Data Center, ESRIN, I-00044 Frascati, Italy. <sup>25</sup>Osservatorio Astronomico di Roma, Via di Frascati 33, I-00040 Monte Porzio Catone, Italy. <sup>26</sup>Agenzia Spaziale Italiana, Viale Liegi 26, I-00198 Roma, Italy.

**Table 1 | Major  $\gamma$ -ray flares of Cyg X-3**

Gamma-ray flaring date	X-ray state	Radio state	$\Delta T_1$ (d)	Radio-flare flux (detection frequency)	$\Delta T_2$ (d)	Gamma-ray flux ( $10^{-8}$ photons $\text{cm}^{-2} \text{s}^{-1}$ )
16–17 April 2008 (MJD = 54,572–54,573)	Soft	Pre-flare	—	$\sim 16$ Jy (11 GHz)	$\sim 0$ –1	$260 \pm 80$
2–3 November 2008 (MJD = 54,772–54,773)	Soft	Pre-quenched	3–4	$\sim 1$ Jy (15 GHz)	$\sim 8$ –9	$258 \pm 83$
11–12 December 2008 (MJD = 54,811–54,812)	Soft	Optically thick–thin change	—	$\sim 3$ Jy (11 GHz)	$\sim 9$ –10	$210 \pm 73$
20–21 June 2009 (MJD = 55,002–55,003)	Soft	Pre-quenched	$\sim 4$ –5	—	—	$212 \pm 75$

Column one shows the dates of the  $\gamma$ -ray flares from Cyg X-3. In all cases, Cyg X-3 showed a low-intensity or non-detectable hard-X-ray flux above 20 keV. Column two shows the X-ray state as determined by the public data in the band (2–12 keV) of the All-Sky Monitor on board NASA's Rossi X-ray Timing Explorer. Column three shows the radio-flare state at the time of the  $\gamma$ -ray flare. Column four shows the time delay,  $\Delta T_1$ , between the  $\gamma$ -ray flare and the radio-state minimum, if applicable. Column five shows the magnitude of the major radio flare following the  $\gamma$ -ray flare (detection radio frequencies given in parentheses). Column six shows the time delay,  $\Delta T_2$ , between the  $\gamma$ -ray flare and the major radio flare. Column seven shows the photon flux of the  $\gamma$ -ray flare above 100 MeV. The errors show the statistical uncertainties and take into account the effects of the Galactic diffuse emission and the presence of nearby sources. MJD, modified Julian date.

significance requirements, implying an occurrence rate for equivalent statistical fluctuations greater than one over several hundred one-day map replications (Supplementary Information). Our values for the flux, significance and position of each of these events are reported in Supplementary Table 1. By integrating all flaring data, we find a transient  $\gamma$ -ray source detected at the  $5.5\sigma$  level at the average Galactic coordinates (longitude, latitude)  $(79.6^\circ, 0.5^\circ) \pm 0.5^\circ_{\text{stat}} \pm 0.1^\circ_{\text{syst}}$  (both types of error apply to both coordinates), with an average flaring flux of  $F = (190 \pm 40) \times 10^{-8}$  photons  $\text{cm}^{-2} \text{s}^{-1}$  above 100 MeV. After careful investigation, we attribute this flaring source to Cyg X-3: no other prominent source is known within the AGILE  $\gamma$ -ray error box. The average spectrum between 100 MeV and 3 GeV is well described by a power law with photon index  $1.8 \pm 0.2$ .

These flares are all associated with special Cyg X-3 radio and X-ray/hard X-ray states. Figure 1 shows the Cyg X-3 daily flux light curve at hard-X-ray energies (15–50 keV) as monitored using the Burst Alert Telescope on board NASA's Swift spacecraft between 1 January 2008 and 30 June 2009. Notably, all  $\gamma$ -ray flares in Table 1 (Fig. 1, red arrows) occur either in coincidence with low hard-X-ray fluxes or during transitions from low hard-X-ray fluxes to high. The Cyg X-3 hard-X-ray fluxes (20 keV and above) and regular-X-ray fluxes (1–10 keV) are anticorrelated<sup>6,12</sup>. Therefore,  $\gamma$ -ray flares occur only during soft-X-ray

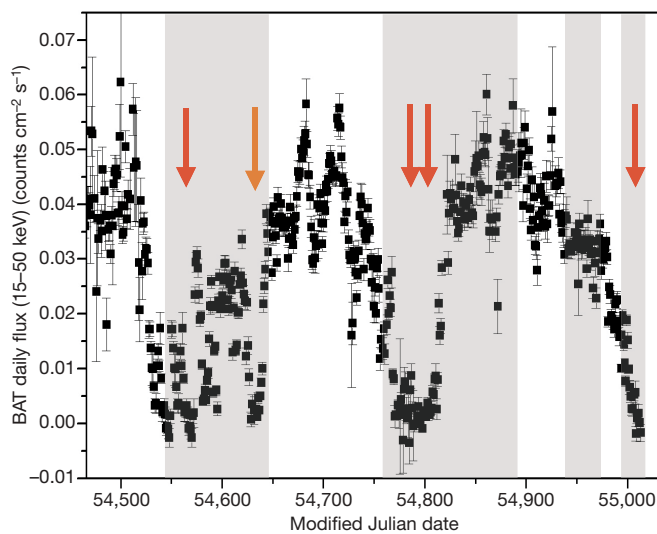


**Figure 1 | Hard-X-ray flux from Cyg X-3 and  $\gamma$ -ray flares.** Daily averaged data (in counts per second in the energy range 15–50 keV) as a function of time, as monitored by the Burst Alert Telescope (BAT) between 1 January 2008 and 25 June 2009 (<http://heasarc.gsfc.nasa.gov/docs/swift/results/transients>). Data errors are 1 s.d. The red arrows mark the dates of major  $\gamma$ -ray flares of Cyg X-3 as detected by the AGILE instrument above 100 MeV and reported in Table 1 (16–17 April 2008, 3–4 November 2008, 20–21 December 2008, 22 June 2009). The orange arrow marks a low-intensity  $\gamma$ -ray flare (20–21 June 2008). Grey areas show the intervals of good AGILE  $\gamma$ -ray exposure of Cyg X-3 with off-axis angles less than  $45^\circ$ .

states or during transitions between such states and quenched hard-X-ray states.

A further crucial piece of information is provided by the Cyg X-3 radio states as monitored by our group using the Arcminute Microkelvin Imager Large Array, UK, and the RATAN-600 radio telescope, Russia. We find that two of four  $\gamma$ -ray flares are distinctly produced before major radio flares. Figure 2 shows the radio,  $\gamma$ -ray, soft-X-ray and hard-X-ray energy data of the strongest radio flare of

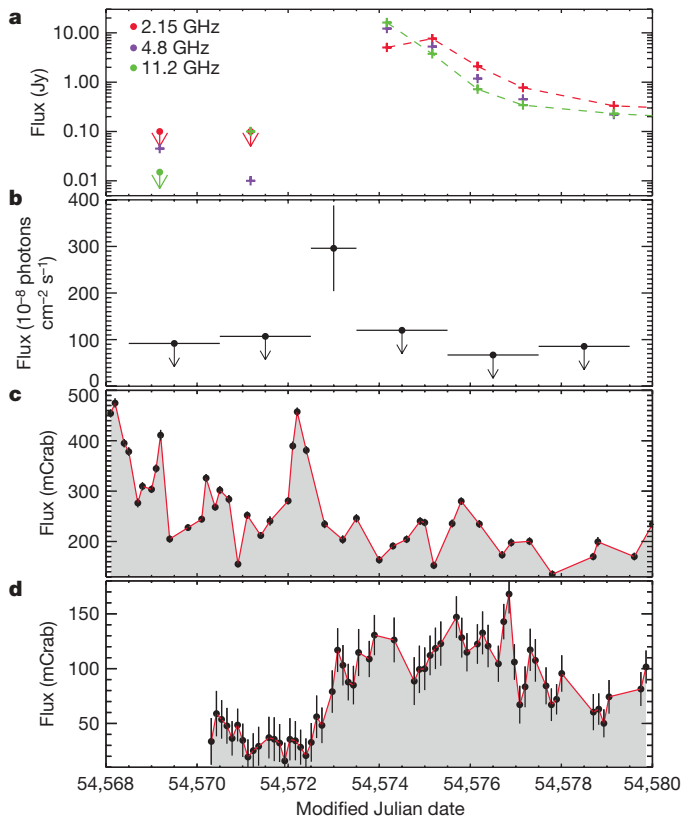


**Figure 2 | Multi-frequency data for Cyg X-3 during the period 13–27 April 2008.** **a**, The major radio flare of Cyg X-3 detected by the RATAN-600 radio telescope. Peak radio emission above 10 Jy at 11 GHz was detected<sup>19</sup> on 18 April 2008 (MJD = 54,574). **b**, Simultaneous AGILE  $\gamma$ -ray monitoring. A major  $\gamma$ -ray flare from a source consistent with Cyg X-3 above 100 MeV is detected  $\Delta T_2 \approx 1$  d before the measured radio peak time. The  $\gamma$ -ray upper limits are at the  $2\sigma$  level. **c**, X-ray flux from Cyg X-3 as monitored by the All-Sky Monitor in the energy band 1.3–12.1 keV (6-h averaged values). The hardness ratio  $F(5$ –12 keV)/ $F(3$ –5 keV) increases by a factor of three on 17 April 2008. **d**, Hard-X-ray flux from Cyg X-3 as monitored quasi-continuously using Super-AGILE (one of the detectors on board AGILE) in the energy range 20–60 keV for an average of 14 observations per day. Errors, 1 s.d.; 1 mCrab corresponds to  $9.3 \times 10^{-12}$  erg  $\text{cm}^{-2} \text{s}^{-1}$  in the 20–60-keV energy range.

our sample (18 April 2008, when Cyg X-3 reached a flux level of 16 Jy at 11 GHz; refs 19, 20). Supplementary Fig. 4 shows the multi-frequency data of the 12 December 2008  $\gamma$ -ray flare, which was also followed by a very strong radio outburst. On 2–3 November 2008 (and probably also on 21–22 June 2009; see Supplementary Figs 3 and 5), the  $\gamma$ -ray activity was associated with the source entering a ‘quenched radio state’<sup>21</sup>, that is, a rare state (occurring 2% of the time) of radio-flux minimum that usually anticipates a major radio flare<sup>8,12</sup>.

Our results show that the flaring  $\gamma$ -ray emission occurs only in special transitional states associated with bright soft-X-ray states and/or the low radio emission that precedes major radio flares. We can clarify this point by using our data to update the schematic view of the radio/X-ray transitions as done in ref. 12. Figure 3 shows the peculiar ‘hysteresis curve’ that Cyg X-3 follows in a radio and soft-X-ray flux diagram representing all spectral states of the source. Remarkably, the  $\gamma$ -ray flares detected by AGILE tend to occur in the ‘gully’ of the hysteresis curve, which corresponds to states of very low radio flux and strong soft-X-ray flux that are preludes to major radio flares. Cyg X-3 spends only a few per cent of its time in these rare states<sup>8,12</sup>.

Our detection of transient  $\gamma$ -ray emission above 100 MeV from Cyg X-3 provides direct evidence that extreme particle acceleration and non-thermalized emission can occur in microquasars with a repetitive pattern. So far, the complex interplay between inner-disk emission (and presumably soft-X-ray emission) and coronal or jet emission (most probably related to hard-X-ray emission) in Cyg X-3 has been addressed by Comptonization models that reproduce<sup>12,13,22</sup> the spectral states up to  $\sim 300$  keV. Despite having a number of important differences with other Galactic systems<sup>22</sup>, the Cyg X-3 states resemble those of accreting black holes with a mixed population of thermal and non-thermal relativistic electrons. The Cyg X-3 X-ray spectral states are fitted by optically thick Comptonized models that include a reflection component<sup>23</sup> and an additional high-energy power-law component<sup>12,13</sup>. Typical temperatures of the hot coronal plasma reach an equivalent energy of  $\sim 10$  keV, and the high-energy

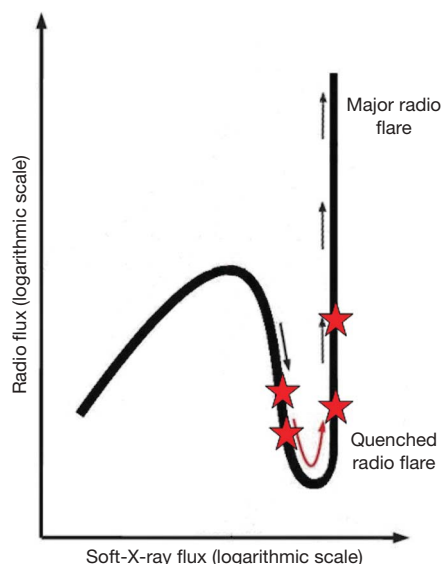


**Figure 3 | Schematic representation of the radio and X-ray spectral states of Cyg X-3.** The trajectory shown represents the correlated radio/soft X-ray spectral states of Cyg X-3 (adapted from ref. 12). The red stars mark the approximate positions of the major  $\gamma$ -ray flares detected by AGILE (Table 1), which tend to occur in low-flux/pre-flare radio states. Cyg X-3 is rarely in these ‘gully’ states (only a few per cent of the total time<sup>8,12</sup>; Supplementary Information). For all  $\gamma$ -ray flaring episodes, the radio and hard-X-ray fluxes are low or very low, whereas the X-ray flux (1–10 keV) is large.

tail has been modelled to extend to photon energies of one megaelectronvolt or slightly higher<sup>12,13</sup>.

However, Cyg X-3 is capable of accelerating particles by a very efficient mechanism leading to photon emission at energies thousands of times larger than the maximum energy so far detected ( $E \approx 300$  keV). Furthermore, photons have to escape from regions that might be opaque to  $\gamma$ -rays because of pair production, unless special conditions are satisfied. The peak  $\gamma$ -ray isotropic luminosity is  $L_\gamma \approx 3 \times 10^{36}$  ergs<sup>-1</sup> above 100 MeV. It is unknown whether this emission is leptonic or hadronic. The site and ultimate origin of this extreme particle acceleration depend on the disk–corona dynamics that lead to jet formation and relativistic propagation. A number of complex phenomena such as coronal magnetic field reconnection or shock acceleration along the proto-jets can take place and influence the formation of particle energy distribution functions at kinetic energies of up to 1 GeV and greater. For leptonic emission (see, for example, refs 24, 25 for microquasar studies), synchrotron radiation in the gigaelectronvolt domain requires large magnetic fields of  $\sim 10^4$  G and Lorentz factors of  $\gamma \approx 10^5$  or greater. Alternatively, inverse Compton emission, at gigaelectronvolt energies, of the soft X-rays from the disk and/or optical or infrared radiation from the companion star also requires Lorentz factors of  $\gamma \approx 10^5$  before being suppressed in the Klein–Nishina regime at teraelectronvolt energies. Depending on the geometry (the Cyg X-3 jet inclination angle is constrained<sup>7</sup> to be  $\sim 10^\circ$ – $20^\circ$ ),  $\gamma$ -ray emission can be boosted or partly suppressed. Hadronic emission involves proton–proton interactions (in the shock-accelerated front interacting, for example, with the Wolf–Rayet mass outflow) in relatively dense environments (see, for example, ref. 26). In this case, protons have to be accelerated to Lorentz factors of  $\gamma \approx 10^2$  or greater, and the interaction may require a critical target density to occur.

Received 7 August; accepted 8 October 2009.

Published online 22 November 2009.

- Krolik, J. H. *Active Galactic Nuclei* (Princeton Univ. Press, 1998).
- Mirabel, I. F. & Rodríguez, L. F. A superluminal source in the galaxy. *Nature* **371**, 46–48 (1994).
- Albert, J. *et al.* Very high energy gamma-ray radiation from the stellar mass black hole binary Cygnus X-1. *Astrophys. J.* **665**, 51–54 (2007).
- Giacconi, R., Gorenstein, P., Gurski, H. & Waters, J. R. An X-ray survey of the Cygnus region. *Astrophys. J.* **148**, L119–L127 (1967).
- Bonnet-Bidaud, J.-M. & Chardin, G. Cygnus X-3, a critical review. *Phys. Rep.* **170**, 325–404 (1988).
- McCullough, M. L. *et al.* Discovery of correlated behavior between the hard X-ray and the radio bands in Cygnus X-3. *Astrophys. J.* **517**, 951–955 (1999).
- Mioduszewski, A. J., Rupen, M. P., Hjellming, R. M., Pooley, G. G. & Waltman, E. B. A one-sided highly relativistic jet from Cygnus X-3. *Astrophys. J.* **553**, 766–775 (2001).
- Waltman, E. B., Friedler, R. L., Johnston, K. J. & Ghigo, F. D. The quiescent level of Cygnus X-3 at 2.25 and 8.3 GHz: 1988–1992. *Astron. J.* **108**, 179–187 (1994).
- Marti, J., Paredes, J. M. & Peracaula, M. The Cygnus X-3 radio jets at arcsecond scales. *Astrophys. J.* **545**, 939–944 (2000).
- Vilhu, O., Hakala, P., Hannikainen, D. C., McCullough, M. & Koljonen, K. Orbital modulation of X-ray emission lines in Cygnus X-3. *Astron. Astrophys.* **501**, 679–686 (2009).
- van Kerkwijk, M. H. *et al.* Infrared helium emission lines from Cygnus X-3 suggesting a Wolf–Rayet star companion. *Nature* **355**, 703–705 (1992).
- Szostek, A., Zdziarski, A. A. & McCullough, M. L. A classification of the X-ray and radio states of Cyg X-3 and their long-term correlations. *Mon. Not. R. Astron. Soc.* **388**, 1001–1010 (2008).
- Hjalmarsdotter, L., Zdziarski, A. A., Szostek, A. & Hannikainen, D. C. Spectral variability in Cygnus X-3. *Mon. Not. R. Astron. Soc.* **392**, 251–263 (2009).
- Tavani, M. *et al.* The AGILE mission. *Astron. Astrophys.* **502**, 995–1013 (2009).
- Giuliani, A. *et al.* Gamma-ray emission from the galaxy: a new model for AGILE. *Mem. Soc. Astron. Ital.* **5**, 135–140 (2004).
- Abdo, A. A., *et al.* Detection of 16 Gamma-Ray Pulsars through blind frequency searches using the Fermi LAT. *Science* **325**, 840–844 (2009).
- Benjamini, Y. & Hochberg, Y. Controlling the false discovery rate – a practical and powerful approach to multiple testing. *J. R. Stat. Soc. A* **57**, 289–300 (1995).
- Miller, C. J. *et al.* Controlling the false-discovery rate in astrophysical data analysis. *Astron. J.* **122**, 3492–3505 (2001).
- Trushkin, S. *et al.* A giant radio flare of Cygnus X-3. *Astron. Teleg.* **1483** (2008).
- Pal, S., Trushkin, S. & Chandra, I. GMRT low frequency radio observation of the giant flare from Cygnus X-3. *Astron. Teleg.* **1486** (2008).
- Pooley, G. Cygnus X-3 radio observations. *Astron. Teleg.* **1828** (2008).

22. Zdziarski, A. A. & Gierlinksi, M. Radiative processes, spectral states and variability of black-hole binaries. *Prog. Theor. Phys.* **155** (suppl.), 99–119 (2004).
23. Coppi, P. S. in *High Energy Processes in Accreting Black Holes* (eds Poutanen, J. & Svensson, R.) 375–403 (ASP Conf. Ser. 161, Astronomy Society of the Pacific, 1999).
24. Atayan, A. M. & Aharonian, F. A. Modelling of the non-thermal flares in the Galactic microquasar GRS 1915+105. *Mon. Not. R. Astron. Soc.* **302**, 253–276 (1999).
25. Markoff, S., Falcke, H. & Fender, R. P. A jet model for the broadband spectrum of XTE J1118+480. Synchrotron emission from radio to X-rays in the low/hard spectral state. *Astron. Astrophys.* **372**, L25–L28 (2001).
26. Romero, G. E., Torres, D. F., Kaufman Bernadó, M. M. & Mirabel, I. F. Hadronic gamma-ray emission from windy microquasars. *Astron. Astrophys.* **410**, L1–L4 (2003).

**Supplementary Information** is linked to the online version of the paper at [www.nature.com/nature](http://www.nature.com/nature).

**Acknowledgements** The AGILE mission is funded by the Italian Space Agency with scientific and programmatic participation by the Italian Institute of Astrophysics and the Italian Institute of Nuclear Physics.

**Author Contributions** M. Tavani, A.B., G. Piano, S.S., E. Striani, G. Pucella and A.G. carried out the  $\gamma$ -ray analysis; G. Pooley, S.T. and N.A.N. obtained and analysed the radio data; and M. McCollough, K.I.I.K., Y.E., E.C. and M.F. analysed and discussed the X-ray data. All authors discussed the results and commented on the manuscript.

**Author Information** Reprints and permissions information is available at [www.nature.com/reprints](http://www.nature.com/reprints). Correspondence and requests for materials should be addressed to M. Tavani ([pi.agile@iasf-roma.inaf.it](mailto:pi.agile@iasf-roma.inaf.it)).